Original Article

Microarray-based gene expression analysis combined with laser capture microdissection is beneficial in investigating the modes of action of ocular toxicity

Makoto Shirai[1*], Noriyo Niino[1], Kazuhiko Mori[2], and Kiyonori Kai[1]

[1] Medicinal Safety Research Laboratories, Daiichi Sankyo Co., Ltd., 1-16-13 Kitakasai, Edogawa-ku, Tokyo 134-0081, Japan
[2] Daiichi Sankyo RD Novare Co., Ltd., 1-16-13 Kitakasai, Edogawa-ku, Tokyo 134-8630, Japan

Abstract: The retina consists of several layers, and drugs can affect the retina and choroid separately. Therefore, investigating the target layers of toxicity can provide useful information pertaining to its modes of action. Herein, we compared gene expression profiles obtained via microarray analyses using samples of target layers collected via laser capture microdissection and samples of the whole globe of the eye of rats treated with *N*-methyl-*N*-nitrosourea. Pathway analyses suggested changes in the different pathways between the laser capture microdissection samples and the whole globe samples. Consistent with the histological distribution of glial cells, up-regulation of several inflammation-related pathways was noted only in the whole globe samples. Individual gene expression analyses revealed several gene expression changes in the laser capture microdissection samples, such as caspase- and glycolysis-related gene expression changes, which is similar to previous reports regarding *N*-methyl-*N*-nitrosourea-treated animals; however, caspase- and glycolysis-related gene expressions did not change or changed unexpectedly in the whole globe samples. Analyses of the laser capture microdissection samples revealed new potential candidate genes involved in the modes of action of *N*-methyl-*N*-nitrosourea-induced retinal toxicity. Collectively, our results suggest that specific retinal layers, which may be targeted by specific toxins, are beneficial in identifying genes responsible for drug-induced ocular toxicity. (DOI: 10.1293/tox.2021-0064; J Toxicol Pathol 2022; 35: 171–182)

Key words: retina, toxic optic neuropathy, laser capture microdissection, microarray analysis, methylnitrosourea, rats

Introduction

Ocular toxicity, including toxicity in the retina and choroid, is a serious problem in the research and development of medical drugs owing to the associated decreased quality of life among patients. The retina is a light receptor tissue of the eye. It consists of several layers, such as the outer nuclear layer (ONL) and the rod and cone photoreceptor layer (PRL)[1, 2]. Each layer is highly specialized; therefore, each layer can be a specific target for retinal toxicants. For example, ethambutol induces selective degeneration of the ganglion cell layer[3], whereas the primary target of sodium iodate is the retinal pigment epithelium[4, 5]. The choroid, which exists under the retinal pigment epithelium and feeds the retina, is a target of toxicity from drugs, such as hydroxychloroquine[6]. The characteristics of layer-specific toxicity in the retina and choroid can make it difficult to investigate the mechanism of ocular toxicity via analyses using whole globe (WG) or striped retina samples owing to dilution of biologically significant signals.

Laser capture microdissection (LCM) has been used to collect target cells and tissues. This technique can be used to overcome the difficulty of investigating molecular changes in each layer of the eye. Microarray-based global gene expression analysis has been widely used to obtain large amounts of transcriptional information on the mechanism of toxicity. Although a combination of these techniques seems preferable in investigating the mechanism of ocular toxicity, such reports are limited.

The purpose of this study was to confirm whether microarray analysis of retinal samples collected via LCM is beneficial compared with analysis of samples from the WG of the eye with the cornea, lens, and vitreous body removed. We compared gene expression levels between these two different samples obtained from rats treated with *N*-methyl-*N*-nitrosourea (MNU), which is known to selectively induce toxicity in the ONL and PRL[7–9]. We also discuss new insights into the mechanism of MNU-induced retinal toxicity.

Materials and Methods

Chemicals, animals, and experimental design

MNU was purchased from Sigma-Aldrich Chemical Co. (St. Louis, MO, USA). Twenty-four 6-week-old male Crl: CD Sprague Dawley rats were obtained from Charles River Laboratories Japan, Inc. (Kanagawa, Japan) and acclimated for 1 week. All rats were fed a normal rodent diet (CRF-1, Oriental Yeast Co., Ltd., Tokyo, Japan) and provided with tap water *ad libitum*. At 7 weeks of age, the rats were given either MNU dissolved in saline containing 0.05% acetic acid (60 mg/kg body weight, n=12) or saline containing 0.05% acetic acid (n=12). After MNU or vehicle dosing, the rats were necropsied at 6 h (n=6 for both the MNU- and vehicle-treated rats) or 7 days (n=6 for both the MNU- and vehicle-treated rats). A dose of 60 mg/kg was selected on the basis of previous reports, in which MNU was administered to female Sprague Dawley rats at or near this dose[8, 10]. The time point of 6 h was set on the basis of previous reports, in which MNU-induced apoptosis in the ONL was completely inhibited by nicotinamide treatment at 4 h after MNU dosing but not at 6 h[10]; this suggested that retinal toxicity due to MNU was irreversible, and some gene expression changes were induced at this time point. The time point of 7 days was used to confirm whether apparent morphological changes were noted in the retina. All experimental procedures were performed in accordance with the in-house guidelines of the Institutional Animal Care and Use Committee of Daiichi Sankyo Co., Ltd. (approval number: A1600654).

Collection of eye samples

At the time of necropsy, all rats were euthanized via exsanguination under anesthesia with isoflurane using an anesthesia apparatus for small animals (MK-A110, Muromachi Kikai Co., Ltd., Tokyo, Japan). After euthanasia, the eyes were collected. The right eyes of the rats necropsied at 6 h after MNU or vehicle dosing were embedded in O.C.T. Compound (Sakura Finetek Japan Co., Ltd., Tokyo, Japan) to prepare the LCM samples (n=3 for both the MNU- and vehicle-treated rats) or frozen in liquid nitrogen to be used as the WG samples after macroscopic removal of the cornea, lens, and vitreous body (n=3 for both the MNU- and vehicle-treated rats). The frozen samples were stored at −80°C for subsequent analysis. The left eyes of the rats necropsied at 6 h and the bilateral eyes of the rats necropsied at 7 days (n=6 for each of the four groups) were fixed with Davidson's fluid and embedded in paraffin for histopathology.

Histopathological examination

Histopathological specimens were prepared from the paraffin-embedded eyes, stained with hematoxylin and eosin, and examined under a light microscope. The noted histopathological changes were graded as 0 (absent), 1 (minimal), 2 (moderate), and 3 (severe) based on the severity and extent of the change, as described below. The reviewing pathologists (K.Y. and A.S.) confirmed the appropriateness of the findings and their grades (grade 0: no apparent changes;

grade 1: less than 20% of the ONL and PRL are affected; grade 2: 20% to 80% of the ONL and PRL are affected; and grade 3: more than 80% of the ONL and PRL are affected).

LCM sampling

Frozen tissue specimens were sectioned at a thickness of 8 μm and mounted on RNAse-free foil slides (Leica Microsystems, Tokyo, Japan). After hematoxylin staining, the ONL and PRL were sampled together using a Leica LMD7000 system (Leica Microsystems). Each sample had an area of 8 mm² or more in total so that microarray analysis could be conducted. To minimize RNA degradation, we limited the time from staining the sections to sampling by LCM to 60 min.

RNA isolation, quantification, and qualification

The WG and LCM samples were homogenized using TRIzol® Reagent (Thermo Fisher Scientific, Carlsbad, CA, USA), and total RNA was isolated. The quality of RNA, including RNA integrity number (RIN), was assessed using a 2100 Bioanalyzer (Agilent Technologies, Santa Clara, CA, USA). The concentration of RNA was assessed using a NanoDrop system (Thermo Fisher Scientific, Inc., Waltham, MA, USA).

Microarray-based gene expression analysis

Complementary DNA and then biotin-labeled complementary RNA were synthesized from the total RNA using the GeneChip® IVT Express kit (Affymetrix, Inc., Santa Clara, CA, USA), in which an oligo-dT primer was contained, according to the manufacturer's instructions. Each biotin-labeled cRNA sample (approximately 10 μg) was individually hybridized to a GeneChip® Rat Genome 230 2.0 Array (Affymetrix, Inc.) at 45°C for 16 h, followed by washing and staining with streptavidin-phycoerythrin using the Fluidics Station 400 (Affymetrix, Inc.). The scanned image was analyzed with the MAS5 algorithm using the GCOS software (Affymetrix, Inc.). All MAS5-analyzed data were scaled via global normalization. Genes whose mean signal intensity values were significantly different from those of the concurrent control with a p-value of <0.05 and whose detection calls were not absent were analyzed using QIAGEN's Ingenuity Pathway Analysis (IPA) software (Qiagen, Tokyo, Japan). Three types of functional analyses using IPA were performed: canonical pathway analysis, upstream regulator analysis, and downstream effector analysis. In the individual gene expression analyses, genes with mean signal intensity values at least 1.2-fold higher/0.83-fold lower than those of the concurrent control were regarded to have significantly changed.

Statistical analysis

In the microarray data analysis, the homogeneity of variance was evaluated using the F test, and the Student's t-test (for homogeneous data) or the Aspin–Welch t-test (for heterogeneous data) was performed using Microsoft Office Excel 2003 (Microsoft, Redmond, WA, USA). In the

canonical pathway, upstream regulator, and downstream effector analyses, the z-score was calculated using IPA. We used conservative criteria with a p-value of <0.05 to judge statistical significance in terms of gene expression and a z-score of ≥2 or ≤−2 to judge significant changes in the IPA functional analyses.

Results

Histopathological examination showed reproducible retinal toxicity by MNU treatment

MNU did not induce any histopathological changes at 6 h after treatment (Table 1 and Fig. 1). However, similar to previous findings[7–9], severe depletion of the ONL and PRL was evident in all MNU-treated rats at 7 days.

RNA from the WG and LCM samples could be used for microarray-based gene expression analysis

To investigate the degree of RNA degradation, we evaluated the RIN. In the WG samples, the RIN ranged from 8.3 to 8.7 (mean: 8.5), while in the LCM samples, it ranged from 3.4 to 6.5 (mean: 4.84); however, the value could not be calculated for one of the LCM samples. Therefore, RNA from the LCM samples was considered to be partially degraded. To confirm whether RNA degradation from the LCM samples affected the results of the microarray analysis, we evaluated the signal intensities of the probes hybridizing the 5 and 3 ends of glyceraldehyde-3-phosphate dehydrogenase (*GAPDH*). As shown in Fig. 2, the signal intensities of *GAPDH* were comparable between the probes at the 5 and 3 ends, and the signal intensity ratio of the probe of the 5 end to that of the 3′ end was 0.8 to 0.9, suggesting that RNA degradation in the LCM samples did not strongly affect the results of the microarray analysis.

Table 1. Histopathological Scores of the Retinal Lesions

Treatment	Vehicle		MNU	
Time after treatment	6 hours	7 days	6 hours	7 days
Number examined	6	6	6	6
Depletion, ONL and PRL[a]	6, 0, 0, 0, 0, 0	6, 0, 0, 0, 0, 0	6, 0, 0, 0, 0, 0	0, 0, 0, 0, 2, 4
Mean score[b]	0	0	0	4.7 ± 0.52

[a] The numbers show the incidences of each grade (0 to 5), with the leftmost number representing grade 0 and the rightmost number indicating grade 5.
[b] The mean of the individual grades.
MNU: *N*-methyl-*N*-nitrosourea; ONL: outer nuclear layer; PRL: rod and cone photoreceptor layer.
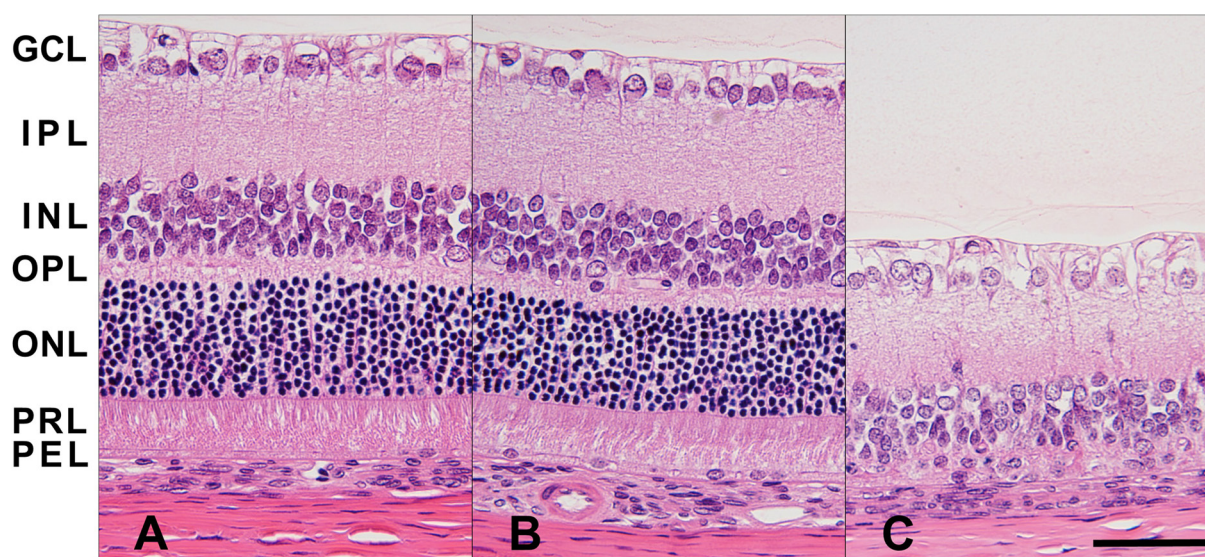
Fig. 1. Histopathological appearance of typical lesions in the retina at 6 h or 7 days after MNU administration.
A: The retina of a rat at 6 h after vehicle treatment. B: The retina of a rat at 6 h after MNU treatment. C: The retina of a rat at 7 days after MNU treatment. No apparent histopathological changes were noted in the retina at 6 h after MNU administration, while the outer nuclear layer and rod and cone photoreceptor layer disappeared at 7 days after MNU administration. GCL, ganglion cell layer; IPL, inner plexiform layer; INL, inner nuclear layer; MNU, *N*-methyl-*N*-nitrosourea; OPL, outer plexiform layer; ONL, outer nuclear layer; PRL, rod and cone photoreceptor layer; PEL, pigment epithelial cell layer. Hematoxylin and eosin staining; bar=50 μm.
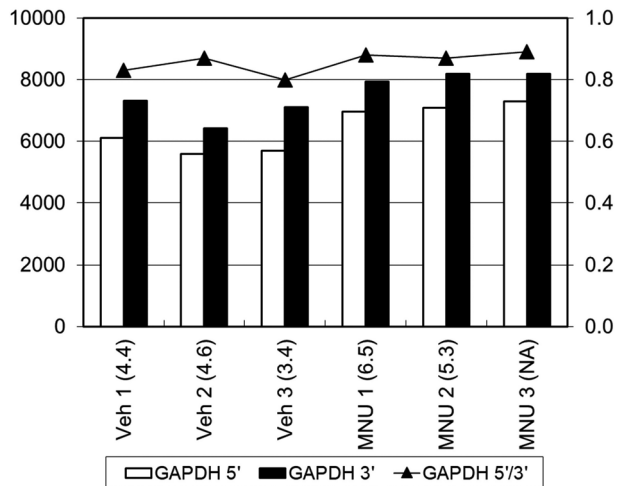
Fig. 2. Signal intensities of the probes hybridizing the 5′ and 3′ ends of *GAPDH* and their ratio in the samples collected via LCM Blank and solid bars indicate the signal intensities of the probes hybridizing the 5′ and 3′ ends, respectively, and the values are indicated by the leftmost numbers. Triangles indicate the ratios of the signal intensities of the probes on the 5′ end to those on the 3′ end, and the values are indicated by the rightmost numbers. The numbers in parentheses at the end of each sample indicate the RNA integrity numbers of the samples. GAPDH, glyceraldehyde-3-phosphate dehydrogenase; LCM, laser capture microdissection.
Veh 1 to 3: Individual LCM samples collected from the vehicle-treated rats (n=3); MNU 1 to 3: Individual LCM samples collected from the MNU-treated rats (n=3).

Table 2. Number of Genes with Expression Level Changes after *N*-methyl-*N*-nitrosourea Treatment

Sample type	Upregulated	Downregulated
LCM sample	1,407	946
WG sample	2,422	2,555

LCM: laser capture microdissection; WG: whole globe of the eye.

Table 3. Significantly Upregulated and Downregulated Pathways in the Canonical Pathway Analysis after MNU Treatment

Predicted pathways	Z-score[a]	
	LCM sample	WG sample
Pathways changed in the LCM sample		
EIF2 signaling	2.9	2.0
RhoA signaling	2.1	NS
NFAT signaling in cardiac hypertrophy	2.0	NS
Pathways changed in the WG sample		
Regulation of actin-based motility by Rho	NS	3.7
iNOS signaling	NS	2.7
Actin nucleation by the ARP-WASP complex	NS	2.7
TREM1 signaling	NS	2.5
Inflammasome signaling	NS	2.4
TNFR1 signaling	NS	2.4
HMGB1 signaling	NS	2.3
Fcγ receptor-mediated phagocytosis in macrophages and monocytes	NS	2.3
Rac signaling	NS	2.3
Osteoarthritis pathway	NS	2.2
Ephrin receptor signaling	NS	2.2
EIF2 signaling	2.9	2.0
PPAR signaling	NS	−2.1

[a] Calculated by comparing gene expression levels between the vehicle- and MNU-treated animals.
MNU: *N*-methyl-*N*-nitrosourea; LCM: laser capture microdissection; WG: whole globe of the eye; NS: not significantly changed; EIF2: eukaryotic initiation factor 2; RhoA: ras homolog gene family member A; NFAT: nuclear factor of activated T cells; iNOS: inducible nitric oxide synthase; ARP-WASP: actin-related protein-Wiskott-Aldrich syndrome protein; TREM1: triggering receptor expressed on myeloid cells 1; TNFR1: tumor necrosis factor receptor 1; HMGB1: high mobility group box-1 protein; PPAR: peroxisome proliferator-activated receptor.

Canonical pathway analysis indicated an inflammatory response in the WG samples

In terms of the number of genes upregulated or downregulated by MNU treatment, the LCM samples showed fewer genes than the WG samples (Table 2). The results of the canonical pathway analysis, which was used to determine which pathways were activated or suppressed in the gene expression profiles by the drug treatment, suggested that the pathways, such as the eukaryotic initiation factor 2 (EIF2) signaling pathway and the ras homolog gene family, member A (RhoA) signaling pathway, were upregulated by MNU treatment in the LCM samples (Table 3). Meanwhile, upregulation of the inflammatory pathways, such as the inducible nitric oxide synthase (iNOS) signaling pathway, triggering receptor expressed on myeloid cells 1 (TREM1) signaling pathway, tumor necrosis factor receptor 1 (TNFR1) signaling pathway, high mobility group box-1 protein (HMGB1) signaling pathway, inflammasome signaling pathway, and a pathway related to Fcγ receptor-mediated phagocytosis in macrophages and monocytes, upregulation of EIF2 signaling, and downregulation of peroxisome proliferator-activated receptor signaling were predicted in the WG samples.

Upstream regulator and downstream effector analyses also suggested differential changes between the LCM and WG samples

The upstream regulator analysis, which was used to indicate the upstream regulators responsible for the observed gene expression profiles, showed different upstream regulators between the LCM and WG samples (Table 4). In the LCM samples, the activating effects of regulators, such as X-box binding protein 1, avian myelocytomatosis viral-related oncogene, neuroblastoma-derived, and fms-related receptor tyrosine kinase 1, and the suppressive effect of regulators, such as mitogen-activated protein kinase kinase kinase kinase 4 and estrogen receptor 1, were suggested by MNU

Table 4. Top 10 Significantly Changed Activated or Suppressed Pathways Predicted in the Upstream Regulator Analysis after MNU Treatment

Predicted upstream regulators	Z-score[a]	
	LCM sample	WG sample
Top 10 regulators predicted in the LCM sample[b]		
XBP1	3.4	NS
PCGEM1	3.3	NS
MYCN	3.1	NS
1,2-Dithiol-3-thione	2.6	NS
miR-200b-3p (and other miRNAs w/ seed AAUACUG)	2.4	NS
ADORA2A	2.4	NS
FLT1	2.4	NS
Galactose	2.2	NS
Metribolone	2.2	NS
miR-8	2.0	NS
ST1926	−5.8	NS
RICTOR	−5.3	NS
CD437	−5.2	NS
5-Fluorouracil	−4.9	NS
MAP4K4	−3.0	NS
ESR1	−2.7	NS
GnRH analog	−2.3	NS
PSEN1	−2.1	NS
TRPC4AP	−2.0	NS
Top 10 regulators predicted in the WG sample		
IFNG	NS	7.3
PDGF BB	NS	6.2
CREB1	NS	6.1
Topotecan	NS	5.6
Salmonella minnesota R595 lipopolysaccharide	NS	4.9
Camptothecin	NS	4.8
TICAM1	NS	4.8
Gentamicin	NS	4.8
MTPN	NS	4.6
AGT	NS	4.3
Sirolimus	NS	−5.1
IRF4	NS	−4.6
LY294002	NS	−4.3
GFI1	NS	−3.9
TSC2	NS	−3.9
Rho	NS	−3.6
SU6656	NS	−3.5
miR-124-3p (and other miRNAs w/ seed AAGGCAC)	NS	−3.5
Alpha catenin	NS	−3.2
Pyridaben	NS	−3.2

[a] Calculated by comparing gene expression levels between the vehicle- and MNU-treated animals.
[b] Only 9 suppressive upstream regulators were predicted in the LCM sample.
MNU: N-methyl-N-nitrosourea; LCM: laser capture microdissection; WG: whole globe of the eye; NS: not significantly changed; XBP1: X-box binding protein 1; PCGEM1: prostate cancer gene expression marker 1; MYCN: avian myelocytomatosis viral related oncogene, neuroblastoma derived; ADORA2A: adenosine A2a receptor; FLT1: fms-related receptor tyrosine kinase 1; RICTOR: rapamycin-insensitive companion of mammalian target of rapamycin; MAP4K4: mitogen-activated protein kinase kinase kinase kinase 4; ESR1: estrogen receptor 1; GnRH: gonadotropin-releasing hormone; PSEN1: presenilin 1; TRPC4AP: transient receptor potential channel 4-associated protein; IFNG: interferon gamma; PDGF BB: platelet-derived growth factor BB; CREB1: cAMP response element binding protein 1; TICAM1: toll-like receptor adaptor molecule 1; MTPN: myotrophin; AGT: angiotensinogen; IRF4: interferon regulatory factor 4; GFI1: growth factor independence 1; TSC2: tuberous sclerosis complex 2.

treatment. Meanwhile, in the WG samples, inflammatory factors were suggested as upstream regulators. The activating effect of an inflammatory cytokine (interferon gamma), an inflammation-associated growth factor (platelet-derived growth factor BB), an adaptor molecule of toll-like receptors (toll-like receptor adaptor molecule 1), and an inflammatory substance (Salmonella minnesota R595 lipopolysaccharide) and the suppressive effect of an adhesion molecule (alpha catenin), Rho, and an immunosuppressant (sirolimus) were predicted in the WG samples.

The downstream effector analysis, which was used to predict the biophysiological effectors led by the gene expression profiles, also suggested different results between the LCM and WG samples (Table 5). In the LCM samples, 9 of the top 10 functions predicted to be activated by MNU treatment were related to infection. Cell death, RNA synthesis, and glycolysis were expected to be suppressed. In the WG samples, functions related to cell survival, proliferation, death, and movement were activated, and the quantity of photoreceptors was suppressed. Moreover, there were no overlapping upstream regulators or downstream biophysiological functions between the LCM and WG samples, at least in the top 10 items.

Genes related to phosphoinositide-3-kinase (PI3K)-AKT and calcium signaling may be differentially expressed between the LCM and WG samples

The results of the canonical pathway and upstream regulator analyses suggested that the inflammatory pathways changed selectively in the WG samples. To understand the differences in further detail, we investigated individual gene expression changes induced by MNU treatment with respect to the genes contained in the iNOS, TREM1, TNFR1, and HMGB1 signaling pathways, the inflammasome pathway, and the pathway related to Fcγ receptor-mediated phagocytosis in macrophages and monocytes, from the canonical pathway analysis using IPA. As shown in Table 6, increased expression levels of phosphoinositide-3-kinase regulatory subunit 2 (*PI3KR2*) and phosphoinositide-3-kinase regulatory subunit 3 (*PI3KR3*) and decreased expression levels of phosphatidylinositol-4-phosphate-3-kinase catalytic subunit type 2 alpha (*PIK3C2A*) and AKT serine/threonine kinase 2 (*AKT2*) were observed in the LCM samples, sug-

Table 5. Top 10 Significantly Changed Activated or Suppressed Pathways Predicted in the Downstream Effector Analysis after MNU Treatment

Predicted downstream effectors	Z-score[a]	
	LCM sample	WG sample
Top 10 effectors predicted in the LCM sample[b]		
Infection of cells	3.3	NS
Infection by RNA virus	3.1	NS
Viral infection	2.8	NS
Infection of embryonic cell lines	2.6	NS
Infection of epithelial cell lines	2.6	NS
Infection of kidney cell lines	2.6	NS
Replication of RNA virus	2.5	NS
HIV infection	2.5	NS
Exocytosis by cells	2.4	NS
Infection by lentivirus	2.4	NS
Synthesis of phosphatidylinositol-4,5-diphosphate	2.2	NS
Death of osteosarcoma cells	−4.6	NS
Initiation of RNA expression	−2.8	NS
Senescence of cells	−2.6	NS
Quantity of cellular protrusions	−2.4	NS
Glycolysis of cells	−2.1	NS
Glycolysis of tumor cell lines	−2.0	NS
Senescence of vascular endothelial cells	−2.0	NS
Top 10 effectors predicted in the WG sample[b]		
Protein kinase cascade	NS	4.2
Cell survival	NS	3.4
Cell viability	NS	3.2
Invasion of tumor cell lines	NS	3.2
Death of cervical cancer cell lines	NS	3.0
Organization of the actin cytoskeleton	NS	2.7
Invasion of cells	NS	2.7
Death of connective tissue cells	NS	2.7
Viability of tumor cell lines	NS	2.5
Oral tumors	NS	2.4
Quantity of photoreceptors	NS	−2.6
Proliferation of thyroid tumor cell lines	NS	−2.0

[a] Calculated by comparing gene expression levels between the vehicle- and MNU-treated animals.
[b] Fewer than 10 suppressed downstream effectors were predicted in both the LCM and WG samples.
MNU: *N*-methyl-*N*-nitrosourea; LCM: laser capture microdissection; WG: whole globe of the eye; NS: not significantly changed.

Table 6. Inflammatory Genes with Significantly Changed Expression Levels in the LCM Sample or Both the LCM Sample and WG Sample after MNU Treatment

Gene	Fold change[a]	
	LCM sample	WG sample
Rab11B, member Ras oncogene family	2.0	NS
Caspase 3	1.8	NS
Actin beta	1.7	NS
Phosphoinositide-3-kinase regulatory subunit 2	1.7	NS
Phosphoinositide-3-kinase regulatory subunit 3	1.6	NS
P21 protein (Cdc42/Rac)-activated kinase 2	1.5	NS
Mitogen-activated protein kinase 9	1.4	NS
Phospholipase A2 group VI	1.4	NS
Ras homolog gene family member A	1.4	NS
Mitogen-activated protein kinase 3	1.4	NS
Protein kinase D3	1.4	NS
NFKB inhibitor beta	1.3	NS
ADP-ribosylation factor 6	1.3	NS
Phosphatidylinositol-4,5-bisphosphate 3-kinase catalytic subunit alpha	1.3	0.8
Ras homolog gene family member T2	1.2	NS
Caspase 9	1.2	0.8
Mitogen-activated protein kinase kinase 6	0.8	NS
CREB binding protein	0.8	1.2
Phosphatidylinositol-4-phosphate 3-kinase catalytic subunit type 2 alpha	0.8	NS
Janus kinase 1	0.8	NS
Phosphatase and tensin homolog	0.8	NS
Mitogen-activated protein kinase kinase kinase 1	0.8	NS
Lymphocyte antigen 96	0.7	NS
AKT serine/threonine kinase 2	0.7	NS
YES proto-oncogene 1, Src family tyrosine kinase	0.7	NS
Fibroblast growth factor receptor substrate 2	0.6	NS
NIMA-related kinase 7	0.6	NS
Actin-related protein 2/3 complex subunit 2	1.7	1.2
Cytochrome C, somatic	1.6	1.2
Calmodulin 1	1.4	1.2
Actin-related protein 2/3 complex subunit 3	1.2	1.3
Lysine acetyltransferase 6A	0.6	NS
Sp1 transcription factor	0.6	0.8
FYN proto-oncogene, Src family tyrosine kinase	0.5	0.8

[a] Calculated by dividing the expression level of the MNU-treated group by that of the vehicle-treated group.
MNU: *N*-methyl-*N*-nitrosourea; LCM: laser capture microdissection; WG: whole globe of the eye; NS: not significantly changed.

gesting the suppression of PI3K-AKT signaling by MNU treatment. In addition, the changes in the mRNA expression levels of cAMP response element binding protein (*CREB*) and calmodulin 1 suggested that MNU affected calcium signaling. Caspase 3 and caspase 9 were also upregulated in the LCM samples. Meanwhile, inflammation-related genes, such as toll-like receptor 4 (*TLR4*), interferon gamma receptor 2, intercellular adhesion molecule 1, tumor necrosis factor receptor superfamily member 1 (*TNFRSF1*) A, tumor necrosis factor receptor superfamily member 11B (*TNFRSF11B*), interleukin 1 receptor type 1 (*IL1R1*), myeloid differentiation primary response 88, nuclear factor kappa B subunit 1 (*NFKB1*), Jun proto-oncogene, AP-1 transcription factor subunit, and Fos proto-oncogene, AP-1 transcription factor subunit were upregulated in the WG samples; meanwhile, most of these genes were unchanged or downregulated in the LCM samples (Tables 6 and 7).

Caspases were discriminatingly expressed in the LCM samples

Given the changes in the expression levels of caspase 3 and caspase 9 in the LCM samples, the expression levels of other caspases were also investigated. In the LCM samples, the mRNA expression levels of caspases other than caspase 3 and caspase 9 remained unchanged (Table 8). In contrast,

Table 7. Inflammatory Genes with Significantly Changed Expression Levels in the WG Sample after MNU Treatment

| Gene | Fold change[a] | |
	LCM sample	WG sample
Fos proto-oncogene, AP-1 transcription factor subunit	NS	3.8
Intercellular adhesion molecule 1	NS	3.0
Signal transducer and activator of transcription 3	NS	2.1
E-selectin	NS	2.0
TNF receptor superfamily member 11B	NS	1.9
TNF receptor superfamily member 1A	NS	1.8
Plasminogen activator, tissue type	NS	1.6
Nerve growth factor receptor	NS	1.6
Rho family GTPase 3	NS	1.5
Interleukin 1 receptor type 1	NS	1.5
Caspase 8	NS	1.5
Interferon regulatory factor 1	NS	1.5
P21 (Rac1) activated kinase 3	NS	1.5
Cd86 molecule	NS	1.5
Jun proto-oncogene, AP-1 transcription factor subunit	NS	1.5
Myeloid differentiation primary response 88	NS	1.4
Caspase 6	NS	1.4
Transforming growth factor-beta 2	NS	1.4
Ras homolog gene family member B	NS	1.4
Caspase 1	NS	1.4
Interleukin-1 receptor-associated kinase 1	NS	1.4
Inositol polyphosphate-5-phosphatase D	NS	1.3
Integrin subunit beta 1	NS	1.3
Receptor-interacting serine/threonine kinase 1	NS	1.3
Nuclear factor kappa B subunit 1	NS	1.3
Interferon gamma receptor 2	NS	1.3
Protein kinase C delta	NS	1.3
Interferon gamma receptor 1	NS	1.2
Cd83 molecule	NS	1.2
Protein kinase C theta	NS	1.2
Interleukin-1 receptor-associated kinase 3	NS	1.2
Rab11A, member Ras oncogene family	NS	1.2
Fc fragment of IgG receptor IIa	NS	1.2
Heme oxygenase 1	NS	1.2
Actin-related protein 2/3 complex subunit 5	NS	1.2
Ras homolog gene family member Q	NS	1.2
Src proto-oncogene, non-receptor tyrosine kinase	NS	1.2
Toll-like receptor 4	NS	1.2
Mitogen-activated protein kinase 8	NS	0.8
KRAS proto-oncogene, GTPase	NS	0.8
MAP kinase-activating death domain	NS	0.8
Protein kinase C beta	NS	0.8
X-linked inhibitor of apoptosis	NS	0.7
Lysine acetyltransferase 2B	NS	0.7
Mitogen-activated protein kinase kinase 5	NS	0.7
Dedicator of cytokinesis 1	NS	0.6
AKT serine/threonine kinase 3	NS	0.6
Protein kinase C alpha	NS	0.6
TNF alpha-induced protein 3	NS	0.5
Class II major histocompatibility complex transactivator	NS	0.5
Talin 2	NS	0.5
Diacylglycerol kinase beta	NS	0.4

[a] Calculated by dividing the expression level of the MNU-treated group by that of the vehicle-treated group.
MNU: *N*-methyl-*N*-nitrosourea; LCM: laser capture microdissection; WG: whole globe of the eye; NS: not significantly changed.

Table 8. Caspases with Significantly Changed Expression Levels in the LCM and/or WG Samples after MNU Treatment

| Caspase | Fold change[a] | |
	LCM sample	WG sample
Caspase 3	1.8	NS
Caspase 9	1.2	0.8
Caspase 1	NS	1.4
Caspase 4	NS	NS
Caspase 6	NS	1.4
Caspase 8	NS	1.5
Caspase 12	NS	1.2

[a] Calculated by dividing the expression level of the MNU-treated group by that of the vehicle-treated group.
MNU: *N*-methyl-*N*-nitrosourea; LCM: laser capture microdissection; WG: whole globe of the eye; NS: not significantly changed.

in the WG samples, the expression level of caspase 3 did not change, while the expression level of caspase 9 showed the opposite change compared with that in the LCM samples. In addition, increased expression levels of caspases 1, 4, 6, 8, and 12 were noted.

Certain genes related to PI3K-AKT and calcium signaling selectively changed in the LCM samples

Since the results of the individual gene expression analyses of the inflammatory genes suggested changes in PI3K-AKT and calcium signaling by MNU treatment in the LCM samples, the genes contained in the signaling pathways from the canonical pathway analysis using IPA were investigated. For the genes related to PI3K-AKT signaling, increased expression levels of phosphatidylinositol-4,5-bisphosphate-3-kinase catalytic subunit alpha (*PIK3CA*) and nuclear factor kappa B inhibitor beta (*IKB*) and decreased expression levels of Janus kinase 1, SOS Ras/Rac guanine nucleotide exchange factor 1, SOS Ras/Rac guanine nucleotide exchange factor 2, and mechanistic target of rapamycin kinase, as well as changes in *PI3KR2*, *PI3KR3*, *PIK3C2A*, and *AKT2* shown in the previous section, were noted in the LCM samples (Tables 6 and 9). In the WG samples, these genes did not change significantly. Meanwhile, upregulation of *NFKB1* and nuclear factor kappa B (*NFKB*) and downregulation of *AKT3*, *PIK3CA*, and the KRAS proto-oncogene, GTPase (*KRAS*), were observed. Investigation of the mRNA expression levels of the genes in the calcium signaling pathway revealed that upregulation of calcium/calmodulin-dependent protein kinase 1 G (*CAMK1G*), calcium/calmodulin-dependent protein kinase 2 beta (*CAMK2B*), calcium/calmodulin-dependent protein kinase 2 gamma (*CAMK2G*), and cAMP response element binding protein 3 (*CREB3*) and downregulation of cAMP response element binding protein 1 (*CREB1*), as well as changes in the expression of CREB binding protein and calmodulin 1 mentioned in the previous section, were noted in the LCM samples (Table 10). In the WG samples, changes in *CAMK1G*, *CAMK2B*, *CAMK2G*, and CREB binding proteins were not observed or were the opposite of those in the LCM

Table 9. PI3K-AKT Signaling-related Genes with Significantly Changed Expression Levels in the LCM and/or WG Samples after MNU Treatment

Gene	Fold change[a]	
	LCM sample	WG sample
Phosphoinositide-3-kinase regulatory subunit 2	1.7	NS
Protein phosphatase 2 scaffold subunit alpha	1.6	NS
Phosphoinositide-3-kinase regulatory subunit 3	1.6	NS
Mdm2 proto-oncogene	1.5	NS
Serine/threonine-protein phosphatase 2A 56 kDa regulatory subunit epsilon isoform	1.4	0.7
Tyrosine 3-monooxygenase/tryptophan 5-monooxygenase activation protein theta	1.4	NS
Mitogen-activated protein kinase 3	1.4	NS
Catenin beta 1	1.3	NS
Heat shock protein 90 alpha family class B member 1	1.3	NS
NFKB inhibitor beta	1.3	NS
Tyrosine 3-monooxygenase/tryptophan 5-monooxygenase activation protein zeta	1.3	NS
Phosphatidylinositol-4,5-bisphosphate 3-kinase catalytic subunit alpha	1.3	NS
Serine/threonine-protein phosphatase 2A 56 kDa regulatory subunit delta isoform	1.2	NS
Janus kinase 1	0.8	NS
Glycogen synthase kinase 3 beta	0.8	NS
Phosphatase and tensin homolog	0.8	NS
Mechanistic target of rapamycin kinase	0.8	NS
AKT serine/threonine kinase 2	0.7	NS
Cyclin-dependent kinase inhibitor 1B	0.7	NS
Protein phosphatase 2 regulatory subunit B alpha	0.7	NS
SOS Ras/Rac guanine nucleotide exchange factor 1	0.7	NS
SOS Ras/Rho guanine nucleotide exchange factor 2	0.7	NS
MCL1, BCL2 family apoptosis regulator	1.4	1.3
Forkhead box O3	0.8	NS
Cyclin-dependent kinase inhibitor 1A	NS	2.0
Prostaglandin-endoperoxide synthase 2	NS	1.8
Mitogen-activated protein kinase kinase kinase 8	NS	1.5
Inositol polyphosphate-5-phosphatase D	NS	1.3
Integrin subunit beta 1	NS	1.3
Synaptojanin 2	NS	1.3
Nuclear factor kappa B subunit 1	NS	1.3
GRB2-associated binding protein 1	NS	1.2
Serine/threonine-protein phosphatase 2A 65 kDa regulatory subunit A beta isoform	NS	1.2
Nuclear factor kappa B subunit 2	NS	1.2
Inositol polyphosphate-5-phosphatase K	NS	1.2
KRAS proto-oncogene, GTPase	NS	0.8
Synaptojanin 1	NS	0.8
Protein phosphatase, Mg2+/Mn2+ dependent 1L	NS	0.7
AKT serine/threonine kinase 3	NS	0.6
Serine/threonine-protein phosphatase 2A 55 kDa regulatory subunit B beta isoform	NS	0.5

[a] Calculated by dividing the expression level of the MNU-treated group by that of the vehicle-treated group.
MNU: *N*-methyl-*N*-nitrosourea; LCM: laser capture microdissection; PI3K: Phosphoinositide-3-kinase; WG: whole globe of the eye; NS: not significantly changed.

Table 10. Calcium Signaling-related Genes with Significantly Changed Expression Levels in the LCM and/or WG Samples after MNU Treatment

Gene	Fold change[a]	
	LCM sample	WG sample
Protein kinase cAMP-activated catalytic subunit beta	1.8	NS
Calcium/calmodulin-dependent protein kinase IG	1.6	NS
Calcium/calmodulin-dependent protein kinase II beta	1.6	NS
Protein kinase cAMP-dependent type I regulatory subunit alpha	1.6	NS
Calcineurin-like EF-hand protein 1	1.5	NS
Protein kinase cAMP-dependent type I regulatory subunit beta	1.4	NS
Mitogen-activated protein kinase 3	1.4	NS
Calcium/calmodulin-dependent protein kinase II gamma	1.3	NS
Calreticulin	1.3	NS
Histone deacetylase 10	1.3	NS
Leucine zipper and EF-hand-containing transmembrane protein 1	1.3	NS
ATPase plasma membrane Ca2+ transporting 1	0.8	NS
CREB binding protein	0.8	1.2
Myocyte enhancer factor 2A	0.8	NS
cAMP responsive element binding protein 1	0.8	NS
Nuclear factor of activated T-cells 5	0.7	NS
Nuclear factor of activated T-cells 3	0.7	NS
ATPase secretory pathway Ca2+ transporting 1	0.7	NS
Protein phosphatase 3 catalytic subunit alpha	0.5	0.8
Tropomyosin 3	1.8	1.4
Calmodulin 1	1.4	1.2
Tropomyosin 4	1.4	1.3
cAMP responsive element binding protein 3	1.3	1.2
E1A binding protein p300	0.8	NS
Tumor protein p63	NS	1.6
cAMP responsive element binding protein 5	NS	1.4
Nuclear factor of activated T-cells 1	NS	1.4
Cholinergic receptor nicotinic beta 4 subunit	NS	1.4
Solute carrier family 8 member B1	NS	1.3
Transient receptor potential cation channel, subfamily C, member 6	NS	1.3
Cholinergic receptor nicotinic alpha 3 subunit	NS	1.2
Rap1B, member of Ras oncogene family	NS	1.2
Protein phosphatase 3 catalytic subunit gamma	NS	0.8
Nuclear factor of activated T-cells 2	NS	0.8
Ryanodine receptor 3	NS	0.7
Solute carrier family 8 member A1	NS	0.7
Glutamate ionotropic receptor AMPA type subunit 3	NS	0.7
Histone deacetylase 8	NS	0.7
Myocyte enhancer factor 2C	NS	0.7
Myosin heavy chain 1	NS	0.7
Glutamate ionotropic receptor kainate type subunit 1	NS	0.6
Glutamate ionotropic receptor kainate type subunit 4	NS	0.6
Calcium/calmodulin-dependent protein kinase II delta	NS	0.6
Ryanodine receptor 2	NS	0.5

[a] Calculated by dividing the expression level of the MNU-treated group by that of the vehicle-treated group.
MNU: *N*-methyl-*N*-nitrosourea; LCM: laser capture microdissection; WG: whole globe of the eye; NS: not significantly changed.

samples. In addition, increased expression levels of cAMP response element binding protein 5 (*CREB5*) and decreased expression levels of calcium/calmodulin-dependent protein kinase 2 delta were noted in the WG samples.

Distinguishable glycolysis-related gene expression changes were observed in the LCM samples

Based on the estimation of the changes in the glycolysis in the LCM samples from the downstream effector analysis, the mRNA expression levels of the genes involved in the glycolysis of cells and the glycolysis of tumor cell lines from the downstream effector analysis were investigated. In the LCM samples, the genes related to glycolysis, such as 6-phosphofructo-2-kinase/fructose-2,6-biphosphatase 2 (*PFKFB2*), hexokinase 2, pyruvate dehydrogenase E1 alpha 1 subunit (*PDHA1*), *GAPDH*, phosphoglucomutase 1

Table 11. Glycolysis-related Genes with significantly Changed Expression Levels in the LCM And/or WG Samples after MNU Treatment

| Gene | Fold change[a] | |
	LCM sample	WG sample
Caveolin 1	2.3	NS
Hexokinase 2	2.0	0.5
O-linked N-acetylglucosamine (GlcNAc) transferase	1.9	NS
ATPase H+ transporting accessory protein 2	1.8	NS
Pyruvate dehydrogenase E1 alpha 1 subunit	1.7	NS
Meningioma expressed antigen 5 (hyaluronidase)	1.7	NS
Basigin (Ok Blood Group)	1.5	NS
6-Phosphofructo-2-kinase/fructose-2,6-biphosphatase 2	1.5	0.8
Glyceraldehyde-3-phosphate dehydrogenase	1.5	NS
Phosphoglucomutase 1	1.4	NS
Branched-chain amino acid transaminase 1	1.4	NS
Complement C1q binding protein	1.4	NS
SUMO1/sentrin/SMT3 specific peptidase 2	1.4	NS
Glucose-6-phosphate isomerase	1.3	NS
CDGSH iron sulfur domain 2	1.3	NS
Cbp/p300 interacting transactivator with Glu/Asp-rich carboxy-terminal domain 2	1.3	NS
Protein kinase AMP-activated catalytic subunit alpha 2	0.8	NS
TERF1-interacting nuclear factor 2	0.8	NS
Glycogen synthase kinase 3 beta	0.8	NS
S-phase kinase-associated protein 2	0.8	NS
Phosphatase and tensin homolog	0.8	NS
Mechanistic target of rapamycin kinase	0.8	NS
Tankyrase 2	0.8	NS
Pyruvate dehyrogenase phosphatase catalytic subunit 1	1.3	1.2
Forkhead box O3	0.8	NS
Tankyrase	0.7	NS
Protein kinase AMP-activated catalytic subunit alpha 1	0.7	NS
Solute carrier family 16 member 3	0.8	0.7
PPARG coactivator 1 alpha	0.7	0.6

[a] Calculated by dividing the expression level of the MNU-treated group by that of the vehicle-treated group.
MNU: *N*-methyl-*N*-nitrosourea; LCM: laser capture microdissection; WG: whole globe of the eye; NS: not significantly changed.

(*PGM1*), glucose-6-phosphate isomerase (*GPI*), and pyruvate dehydrogenase phosphatase catalytic subunit 1 (*PDP1*) were upregulated, while glycogen synthase kinase 3 beta (*GSK3B*) was downregulated (Table 11). Most of these genes were unchanged or downregulated in the WG samples.

Discussion

Ocular toxicity profoundly worsens patients' quality of life, and once it occurs, it becomes a serious problem in the research and development of medical drugs. The retina consists of several thin layers, which can be separately affected by drug toxicity[5–8]; therefore, more useful information can be obtained by investigating target layers compared with the homogenate of the WG of the eye or retina. Because it is difficult to separately collect each layer of the retina manually, except when it comes to the retinal pigment epithelium[11], LCM, which is an established technique for collecting the intended part of the tissues from histopathological sections, is considered to be beneficial when investigating the modes of action (MOA) of ocular toxicities. Herein, we investigated whether microarray analysis of target retinal layers collected via LCM could be used to detect reproducible changes due to MNU toxicity in line with previous studies and obtain additional information to speculate on the MOA of retinal toxicity compared with the analysis of WG samples.

First, the reproducibility of retinal toxicity due to MNU treatment was confirmed. All of the rats in this study showed severe depletion of the ONL and PRL at 7 days after treatment with 60 mg of MNU, which is similar to previous findings[7–9]. Therefore, significant gene profile changes were considered to be induced in all of the samples at 6 h after the treatment, at which time the samples for the microarray analysis were obtained, as MNU-induced retinal toxicity became irreversible at this time point[10]. Second, the RNA integrity was confirmed by the RIN; however, the RIN ranged from 3.4 to 6.5 (mean: 4.84) in the LCM samples, and RNA degradation was suspected. Hence, we investigated the signal intensities of the different probes for *GAPDH* with reference to the 3′:5′ assay on *GAPDH* to confirm the RNA integrity; this is based on the logic that with oligo-dT primer, cDNA can be synthesized only from the mRNA with poly(A), so the possibility of cDNA synthesis from the mRNA sequence near the 3′ end (poly[A] side) should be higher than the 5′ end if mRNA is degraded[12]. As a result, the ratio of the signal intensity of the probe on the 5 end to that on the 3′ end of *GAPDH* was 0.8 to 0.9 in the LCM samples, suggesting that degradation was unbiased in the RNA sequence and therefore did not affect the relative gene expression intensity among the genes. Indeed, it has been reported that formalin-fixed samples, whose RIN was lower than that of the LCM samples in our study (2.2 to 2.4), showed gene expression profiles similar to those of frozen samples with a higher RIN (n=3, Pearson's correlation coefficient=0.876–0.904)[13]. Therefore, the RNA degradation noted in the LCM samples was judged to have limited substantial effect on the gene expression profiles, and the

microarray-based gene expression analysis was continued.

The comparison of the gene expression changes induced by MNU treatment revealed clearly different profiles between the LCM and WG samples. For example, the canonical pathway analysis, upstream regulator analysis, and biophysiological effector analysis predicted mostly non-overlapping pathways. In particular, inflammatory pathways were notably predicted in the WG samples but not in the LCM samples; therefore, one of the major differences in the gene expression changes between the LCM and WG samples would be expected to be related to inflammatory genes. Indeed, the individual analyses of inflammatory gene expression changes demonstrated that the genes related to PI3K-AKT signaling were upregulated in the LCM samples, while the expression levels of genes, such as *TLR4, TNFRSF1, TNFRSF11B*, and *IL1R1*, increased in the WG samples. MNU treatment activates Müller cells, which are glial cells in the retina, and Müller cells express toll-like receptors, such as *TLR4*, and produce cytokines, such as TNF-α and interleukin-1β[14–16]. The cytosol of Müller cells exists from the outer limiting membrane to the inner limiting membrane, including the ONL, but not the PRL[14, 15]. In addition, the retinal pigment epithelium produces various cytokines[17], and treatment with ultraviolet-irradiated photoreceptor outer segments and human complement sera results in increased cytokine production[18]. Therefore, it is speculated that the changes in the inflammatory gene expression selectively noted in the WG samples arose from Müller cells and/or the retinal pigment epithelium, which do not exist in the main target layers of MNU toxicity; further, the gene expression changes noted only in the LCM samples were considered to be more useful in speculating on the MOA of toxicity.

Apoptosis in photoreceptor cells has been noted in MNU-treated rats at 24 h and was completed by 7 days after treatment[8], and caspases have been reported to be involved in retinal degeneration caused by MNU[9, 19]. In this study, the gene expression profiles of the LCM and WG samples were different. In the LCM samples, caspases 3 and 9 were upregulated. Caspase 3 is activated by caspase 9[20, 21], and a caspase 3 inhibitor weakens MNU-induced retinal toxicity in rats[9]; therefore, the increased expression levels of caspase 3 and caspase 9 in the ONL and PRL were considered to be related to MNU-induced retinal toxicity. Meanwhile, in the WG samples, there were no apparent changes in caspase 3, while caspase 9 was downregulated. In addition, increased expression levels of caspases 1, 6, 8, and 12, which are related to inflammation and/or microglial activation[21–24], were also noted. Hence, in the WG samples, changes in the expression of caspases related to inflammatory reactions may have been apparent since these samples contained Müller cells and retinal pigment epithelium, while specific changes, such as increases in the expression of caspases 3 and 9, could not be detected in the target retinal layers.

Individual gene analyses showed changes in the expression of genes related to PI3K-AKT signaling in both the LCM and WG samples. Although the changes in *PIK3C*

and *AKT* were shared, upregulation of *IKB*, a suppressor of NFKB[25], was observed only in the LCM samples, while an increased expression level of *NFKB* was noted only in the WG samples. In the MNU-treated rats in the study by Miki *et al.*, the level of phospho-NFKB significantly decreased, and the level of phosphorylated IKB did not significantly change in the homogenate of the whole retina[26]; therefore, NFKB activity is suspected to contribute to MNU-induced retinal toxicity. Hence, our results showed the possibility that the ONL/PRL-specific decrease in *IKB* expression contributes to the suppression of NFKB signaling and retinal toxicity caused by MNU.

In addition to PI3K-AKT signaling, calcium signaling was also suggested to be affected by MNU treatment. Upregulation of calmodulin and calcium/calmodulin-dependent protein kinase (*CAMK*) was observed in the LCM samples, while upregulation of calmodulin and downregulation of *CAMK* were noted in the WG samples. *CAMK2*, a kinase activated by calmodulin, leads to an apoptosis response[27]. Glutamate has been shown to decrease cell viability in a differentiated human retinoblastoma-derived cell line and increase *CAMK2* activity[28]. Furthermore, a mouse model harboring a mutation in a rod photoreceptor-specific phosphodiesterase gene with rapid degeneration of the cells has been shown to increase *CAMK2* activity[29]. Based on these data, it is possible that ONL- and PRL-specific increases in the gene expression levels of calmodulin and *CAMK* contribute to MNU-induced retinal toxicity.

The IPA downstream effector analysis predicted changes in glycolysis, and the individual gene analysis demonstrated increased expression levels of the glycolysis-related genes, such as *HX1, PDHA1, GAPDH, PGM1, GPI, PFKFB2*, and *PDP1*, as well as decreased expression levels of *GSK3B* in the LCM samples, but not in the WG samples. MNU becomes a DNA adduct to become toxic, and DNA adducts are formed specifically in the ONL in MNU-treated rats[19, 30]. DNA adduct formation induces poly (ADP-ribose) polymerase, which results in adenosine triphosphate (ATP) depletion by using nicotinamide adenine dinucleotide for DNA repairment[19]. Additionally, decreased glycogen and increased glycolysis enzymes, such as hexokinase, glucose-6-phosphatase, and glucose-6-isomerase, are induced by MNU in the brains of mice, suggesting complementary glucose metabolism, including glycolysis, to synthesize ATP[31]. Hence, the upregulation of the glycolysis-related genes selectively noted in the LCM samples was considered to be a reactive change against DNA adduct formation in the ONL by MNU treatment. Meanwhile, the expression of *GSK3B*, which encodes an inhibitory enzyme of glycogen synthesis[32, 33], was suppressed, while no change in glycogen synthetase expression was noted in the LCM samples. Therefore, decreased *GSK3B* expression may increase glycogen synthesis by interrupting the complimentary glycolysis against MNU toxicity. Moreover, it has been reported that GSK3B activity in the retina of MNU-treated rats decreased and that GSK3B activator treatment ameliorated MNU-induced retinal toxicity[34]. Collectively, it is speculated that

one of the MOA of MNU-induced retinal toxicity is the inhibition of glycolysis for ATP supplementation by increased glycogen synthesis due to decreased *GSK3B* expression in the ONL and PRL.

Although we evaluated the usefulness of a combination of retinal layer sampling via LCM and microarray analysis, there are alternatives for collecting samples and investigating retinal layer-specific transcriptome changes. Separately collecting each layer of the retina manually under a light microscope immediately after necropsy can obtain more intact RNA than using LCM, as shown by the higher RIN of the WG samples in this study, although it is difficult to perform, except for the retinal pigment epithelium[11]. Single-cell RNA sequencing technologies may provide more detailed and precise bioinformatics information of individual cells in target layers than the method used in our study; however, it takes a longer time to establish optimal methods to collect each cell, optimize and standardize analytical protocols, and interpret large amounts of data[35]. Considering that retinal toxicity is mostly unexpected and rapid investigation would be required, especially when toxicity is induced in studies for developing drugs, the combination of LCM sampling and microarray analysis is considered to be the first selected method owing to the high flexibility of LCM sampling and well-established methods of microarray analysis during almost 20 years of history[35].

As mentioned above, we judged that the RNA quality measured by the RIN was acceptable for microarray analysis; however, there may be several methods to improve the RNA quality of LCM samples obtained from the retina. We performed sampling via LCM at room temperature; thus, the RNA in the section was considered to be degrading during sampling. If this process can be performed in a cold room, RNA degradation should be reduced. In addition, considering the throughput to collect samples at once, the working time from staining sections to collecting samples via LCM was set as 60 min at maximum in our study. Higher-quality samples may be obtained if the maximum working time is shortened. Hematoxylin staining was used as the staining method. This was determined in the in-house preliminary trials comparing the RNA quality of samples stained by hematoxylin to toluidine blue, which is recommended in the manufacturer's instructions (data not shown); however, there may be room for optimizing the staining method to obtain high-quality RNA samples.

In conclusion, our results suggest that LCM and microarray investigations of selective toxicity of specific retinal layers may be useful in analyzing the MOA of retinal toxicity, although RNA degradation may occur during sample preparation and/or collection via LCM. The MNU-induced gene expression changes noted in the LCM samples, such as those involving caspase- and glycolysis-related genes, were similar to those previously reported in MNU-treated animals. Moreover, the analyses of the LCM samples revealed new potential candidates involved in the MOA of MNU-induced retinal toxicity, such as upregulation of the *IKB* and *CAMK* genes, and inhibition of glycolysis by decreasing

GSK3B gene expression. Most of these changes were not detected in the WG samples. Collectively, our results strongly suggest that microarray analysis of specific LCM-collected retinal layers, which may be affected by specific toxins, is beneficial and that it is possible to find MOA-related genes, which cannot be detected in the analysis of WG samples.

References

1. Lee GI, Park KA, Son G, Kong DS, and Oh SY. Optical coherence tomography analysis of inner and outer retinal layers in eyes with chiasmal compression caused by suprasellar tumours. Acta Ophthalmol. **98**: e373–e380. 2020. [Medline] [CrossRef]
2. Werner JS, Keltner JL, Zawadzki RJ, and Choi SS. Outer retinal abnormalities associated with inner retinal pathology in nonglaucomatous and glaucomatous optic neuropathies. Eye (Lond). **25**: 279–289. 2011. [Medline] [CrossRef]
3. Heng JE, Vorwerk CK, Lessell E, Zurakowski D, Levin LA, and Dreyer EB. Ethambutol is toxic to retinal ganglion cells via an excitotoxic pathway. Invest Ophthalmol Vis Sci. **40**: 190–196. 1999. [Medline]
4. Kiuchi K, Yoshizawa K, Shikata N, Moriguchi K, and Tsubura A. Morphologic characteristics of retinal degeneration induced by sodium iodate in mice. Curr Eye Res. **25**: 373–379. 2002. [Medline] [CrossRef]
5. Kannan R, and Hinton DR. Sodium iodate induced retinal degeneration: new insights from an old model. Neural Regen Res. **9**: 2044–2045. 2014. [Medline] [CrossRef]
6. Ahn SJ, Ryu SJ, Joung JY, and Lee BR. Choroidal thinning associated with hydroxychloroquine retinopathy. Am J Ophthalmol. **183**: 56–64. 2017. [Medline] [CrossRef]
7. Emoto Y, Yoshizawa K, Kinoshita Y, Yuki M, Yuri T, and Tsubura A. Susceptibility to N-methyl-N-nitrosourea-induced retinal degeneration in different rat strains. J Toxicol Pathol. **29**: 67–71. 2016. [Medline] [CrossRef]
8. Nakajima M, Yuge K, Senzaki H, Shikata N, Miki H, Uyama M, and Tsubura A. Photoreceptor apoptosis induced by a single systemic administration of N-methyl-N-nitrosourea in the rat retina. Am J Pathol. **148**: 631–641. 1996. [Medline]
9. Yoshizawa K, Yang J, Senzaki H, Uemura Y, Kiyozuka Y, Shikata N, Oishi Y, Miki H, and Tsubura A. Caspase-3 inhibitor rescues N-methyl- N-nitrosourea-induced retinal degeneration in Sprague-Dawley rats. Exp Eye Res. **71**: 629–635. 2000. [Medline] [CrossRef]
10. Kiuchi K, Yoshizawa K, Shikata N, Matsumura M, and Tsubura A. Nicotinamide prevents N-methyl-N-nitrosourea-induced photoreceptor cell apoptosis in Sprague-Dawley rats and C57BL mice. Exp Eye Res. **74**: 383–392.

2002. [Medline] [CrossRef]

11. Shang P, Stepicheva NA, Hose S, Zigler JS Jr, and Sinha D. Primary cell cultures from the mouse retinal pigment epithelium. J Vis Exp. **133**: e56997. 2018. [Medline]

12. Nolan T, Hands RE, and Bustin SA. Quantification of mRNA using real-time RT-PCR. Nat Protoc. **1**: 1559–1582. 2006. [Medline] [CrossRef]

13. Wimmer I, Tröscher AR, Brunner F, Rubino SJ, Bien CG, Weiner HL, Lassmann H, and Bauer J. Systematic evaluation of RNA quality, microarray data reliability and pathway analysis in fresh, fresh frozen and formalin-fixed paraffin-embedded tissue samples. Sci Rep. **8**: 6351. 2018. [Medline] [CrossRef]

14. Coorey NJ, Shen W, Chung SH, Zhu L, and Gillies MC. The role of glia in retinal vascular disease. Clin Exp Optom. **95**: 266–281. 2012. [Medline] [CrossRef]

15. Fernández-Sánchez L, Lax P, Campello L, Pinilla I, and Cuenca N. Astrocytes and Müller cell alterations during retinal degeneration in a transgenic rat model of retinitis pigmentosa. Front Cell Neurosci. **9**: 484. 2015. [Medline] [CrossRef]

16. Nomura-Komoike K, Saitoh F, Komoike Y, and Fujieda H. DNA damage response in proliferating Müller glia in the mammalian retina. Invest Ophthalmol Vis Sci. **57**: 1169–1182. 2016. [Medline] [CrossRef]

17. Kumar A, Pandey RK, Miller LJ, Singh PK, and Kanwar M. Muller glia in retinal innate immunity: a perspective on their roles in endophthalmitis. Crit Rev Immunol. **33**: 119–135. 2013. [Medline] [CrossRef]

18. Lueck K, Hennig M, Lommatzsch A, Pauleikhoff D, and Wasmuth S. Complement and UV-irradiated photoreceptor outer segments increase the cytokine secretion by retinal pigment epithelial cells. Invest Ophthalmol Vis Sci. **53**: 1406–1413. 2012. [Medline] [CrossRef]

19. Tsubura A, Lai YC, Miki H, Sasaki T, Uehara N, Yuri T, and Yoshizawa K. Review: Animal models of N-Methyl-N-nitrosourea-induced mammary cancer and retinal degeneration with special emphasis on therapeutic trials. In Vivo. **25**: 11–22. 2011. [Medline]

20. Porter AG, and Jänicke RU. Emerging roles of caspase-3 in apoptosis. Cell Death Differ. **6**: 99–104. 1999. [Medline] [CrossRef]

21. Fan TJ, Han LH, Cong RS, and Liang J. Caspase family proteases and apoptosis. Acta Biochim Biophys Sin (Shanghai). **37**: 719–727. 2005. [Medline] [CrossRef]

22. Berta T, Lee JE, and Park CK. Unconventional role of caspase-6 in spinal microglia activation and chronic pain. Mediators Inflamm. **2017**: 9383184. 2017. [Medline] [CrossRef]

23. García de la Cadena S, and Massieu L. Caspases and their role in inflammation and ischemic neuronal death. Focus on caspase-12. Apoptosis. **21**: 763–777. 2016. [Medline] [CrossRef]

24. Monie TP, and Bryant CE. Caspase-8 functions as a key

25. mediator of inflammation and pro-IL-1β processing via both canonical and non-canonical pathways. Immunol Rev. **265**: 181–193. 2015. [Medline] [CrossRef]

25. Nolan GP, Ghosh S, Liou HC, Tempst P, and Baltimore D. DNA binding and I kappa B inhibition of the cloned p65 subunit of NF-kappa B, a rel-related polypeptide. Cell. **64**: 961–969. 1991. [Medline] [CrossRef]

26. Miki K, Uehara N, Shikata N, Matsumura M, and Tsubura A. Poly (ADP-ribose) polymerase inhibitor 3-aminobenzamide rescues N-methyl-N-nitrosourea-induced photoreceptor cell apoptosis in Sprague-Dawley rats through preservation of nuclear factor-kappaB activity. Exp Eye Res. **84**: 285–292. 2007. [Medline] [CrossRef]

27. Brnjic S, Olofsson MH, Havelka AM, and Linder S. Chemical biology suggests a role for calcium signaling in mediating sustained JNK activation during apoptosis. Mol Biosyst. **6**: 767–774. 2010. [Medline] [CrossRef]

28. Wang K, Zhu X, Zhang K, Wu Z, Sun S, Zhou F, and Zhu L. Neuroprotective effect of puerarin on glutamate-induced cytotoxicity in differentiated Y-79 cells via inhibition of ROS generation and Ca(2+) influx. Int J Mol Sci. **17**: 1109. 2016. [Medline] [CrossRef]

29. Hauck SM, Ekström PA, Ahuja-Jensen P, Suppmann S, Paquet-Durand F, van Veen T, and Ueffing M. Differential modification of phosducin protein in degenerating rd1 retina is associated with constitutively active Ca2+/calmodulin kinase II in rod outer segments. Mol Cell Proteomics. **5**: 324–336. 2006. [Medline] [CrossRef]

30. Ogino H, Ito M, Matsumoto K, Yagyu S, Tsuda H, Hirono I, Wild CP, and Montesano R. Retinal degeneration induced by N-methyl-N-nitrosourea and detection of 7-methyldeoxyguanosine in the rat retina. Toxicol Pathol. **21**: 21–25. 1993. [Medline] [CrossRef]

31. Singla N, and Dhawan DK. Modulation of carbohydrate metabolism during N-methyl N-nitrosourea induced neurotoxicity in mice: role of curcumin. Neurochem Res. **35**: 660–665. 2010. [Medline] [CrossRef]

32. Cohen P, and Goedert M. GSK3 inhibitors: development and therapeutic potential. Nat Rev Drug Discov. **3**: 479–487. 2004. [Medline] [CrossRef]

33. Summers SA, Kao AW, Kohn AD, Backus GS, Roth RA, Pessin JE, and Birnbaum MJ. The role of glycogen synthase kinase 3beta in insulin-stimulated glucose metabolism. J Biol Chem. **274**: 17934–17940. 1999. [Medline] [CrossRef]

34. Wang B, Hu C, Yang X, Du F, Feng Y, Li H, Zhu C, and Yu X. Inhibition of GSK-3β activation protects SD rat retina against N-methyl-N-nitrosourea-induced degeneration by modulating the Wnt/β-catenin signaling pathway. J Mol Neurosci. **63**: 233–242. 2017. [Medline] [CrossRef]

35. Rao MS, Van Vleet TR, Ciurlionis R, Buck WR, Mittelstadt SW, Blomme EAG, and Liguori MJ. Comparison of RNA-seq and microarray gene expression platforms for the toxicogenomic evaluation of liver from short-term rat toxicity studies. Front Genet. **9**: 636. 2019. [Medline] [CrossRef]